Anisotropic elastic properties of nanocrystalline nickel thin films

D.C. Hurley,[a] R.H. Geiss, M. Kopycinska-Müller, J. Müller, D.T. Read, and J.E. Wright
Materials Reliability Division, National Institute of Standards & Technology, Boulder, Colorado 80305

N.M. Jennett and A.S. Maxwell
Materials Centre, National Physical Laboratory, Teddington, Middlesex TW11 0LW, United Kingdom

(Received 5 October 2004; accepted 26 January 2005)

The elastic properties of a nickel film approximately 800 nm thick were measured with nanoindentation, microtensile testing, atomic force acoustic microscopy (AFAM), and surface acoustic wave (SAW) spectroscopy. Values for the indentation modulus (220–223 GPa) and Young's modulus (177–204 GPa) were lower than predicted for randomly oriented polycrystalline nickel. The observed behavior was attributed to grain-boundary effects in the nanocrystalline film. In addition, the different measurement results were not self-consistent when interpreted assuming elastic isotropy. Agreement was improved by adopting a transversely isotropic model corresponding to the film's ⟨111⟩ preferred orientation and reducing the elastic moduli by 10–15%. The SAW spectroscopy results indicated that the film density was 1–2% lower than expected for bulk nickel, consistent with models for nanocrystalline materials. Similar reductions in modulus and density were observed for two additional films approximately 200 and 50 nm thick using AFAM and SAW spectroscopy. These results illustrate how complementary methods can provide a more complete picture of film properties.

I. INTRODUCTION

As the usefulness and applicability of thin films continues to expand, increasingly more detailed information about them is needed. In particular, many applications require knowledge about a film's mechanical behavior to predict or diagnose its performance in a product. Several techniques based on a variety of physical principles have accordingly been developed to evaluate the mechanical properties of thin films.[1–4] Although all of these techniques provide useful information, the measured properties often differ from one another. The question of how well the disparate measurements agree to form a unified, consistent picture of a film's properties has not yet been fully answered.

In this paper, we compare measurements of the elastic properties of thin films obtained by four very different measurement methods. Methods included nanoindentation, microtensile testing, surface acoustic wave spectroscopy, and atomic force acoustic microscopy. The methods spanned several orders of magnitude in their spatial resolution, from the macroscale to the nanoscale. Some of the methods were nondestructive; others permanently damaged the sample. Some measurements were performed under quasistatic conditions; others involved acoustic vibrations at frequencies greater than 100 MHz. In spite of their differences, all four methods provide valuable information about a film's properties. By combining and comparing measurement results,[5] we can obtain a more complete picture of the film's properties, including density and thickness as well as elastic moduli. Specifically, we show how our results lead us to interpret the film using an elastically anisotropic model. Although somewhat more complicated than simple isotropic elasticity, the model is more physically realistic and is compatible with all of the available information.

We have used nickel (Ni) as the film material in this work. Micro- and nanostructured nickels possess technological significance for several applications, such as corrosion or wear resistant coatings, contact layers in microelectronic circuitry, and as a potential alternative to silicon in microelectromechanical systems (MEMS) devices.[6,7] For such applications, information about the properties of nickel films may assist in the modeling and prediction of mechanical behavior. There is also interest in nickel as a platform with which to explore the relation

[a]Address all correspondence to this author.
e-mail: hurley@boulder.nist.gov
DOI: 10.1557/JMR.2005.0146

between strength or hardness and grain size for nanometer-sized grains.[8]

II. EXPERIMENTAL TECHNIQUES

A. Sample preparation and characterization

The sample used in these experiments was a Ni film sputtered onto a (001) single-crystal silicon (Si) substrate using room-temperature direct current (dc) magnetron techniques. The native oxide layer on the wafer was removed by etching prior to film deposition. Different segments of the same wafer were used for all of the different experiments described below. The nominal film thickness was 800 nm; its actual thickness was determined from calibrated scanning electron microscope (SEM) images of the sample in cross section. From six measurements at various places on the sample, the value $t = 772 \pm 5$ nm was obtained for the average film thickness. The uncertainty in t was based on the scatter in individual measurements.

X-ray diffraction (XRD) methods were used to assess the preferred grain orientation of the Ni film. The measured XRD spectrum shown in Fig. 1 contained a strong peak at a 2θ-angle of 44.6° and a weaker peak at 98.7°, corresponding to the ⟨111⟩ and ⟨222⟩ orientation of single-crystal Ni, respectively. The full width at half maximum of the ⟨111⟩ peak was determined by a split-Pearson VII-function analysis and found to be 0.4°. Although our spectral analysis of the XRD peaks was only qualitative, it clearly indicated that the film grain size was quite small. Quantitative information about the film's microstructure was obtained by SEM analysis. Figure 2 shows SEM images of the film. The cross-sectional image in Fig. 2(a) indicates that the crystallites

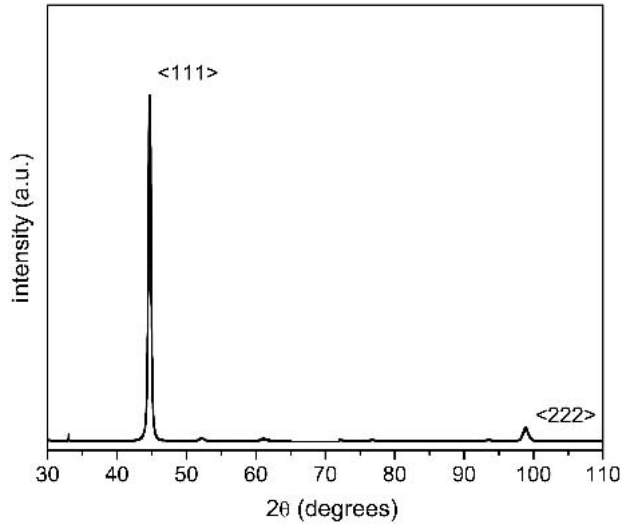

FIG. 1. XRD spectrum of sputtered Ni film 772 nm thick. The (001) Si peak has been removed from the spectrum.

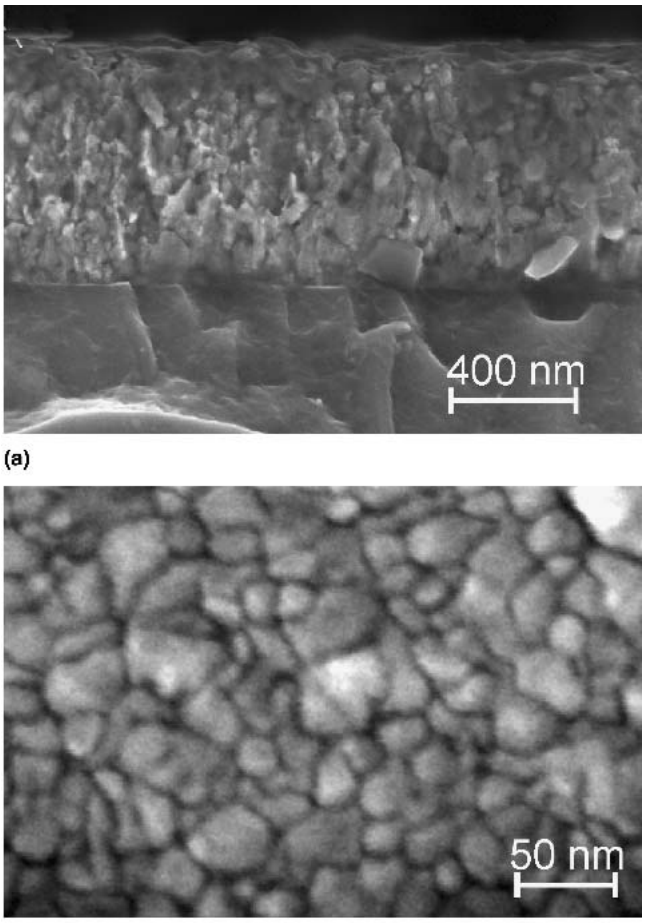

FIG. 2. SEM images of sputtered Ni film 772 nm thick: (a) cross-sectional view and (b) top view.

are approximately equiaxed. The plan-view image in Fig. 2(b) shows a few relatively large grains (diameter 40–50 nm), but grains with diameter 20–30 nm dominate the surface topography. Use of commercial image analysis software to estimate the grain size revealed that the average grain diameter $d = 27 \pm 10$ nm. From the XRD and SEM results, we concluded that the film was nanocrystalline.

B. Microtensile testing

Microtensile experiments were performed using force-probe techniques previously described.[9] Unlike the methods described below that used blanket film samples, the microtensile experiments required a specialized specimen geometry. The specimen was essentially a miniaturized version of a conventional tensile test specimen, with a gage section of freestanding thin film approximately $190 \times 4.7 \times 0.77$ μm^3 in size. Specimens were prepared from a section of the original film/substrate sample by photolithographic processing and etch release of the film. The specimen was loaded by a pin mounted on an

instrumented force probe with a built-in force sensor that had been calibrated against a force pendulum. Engineering strain was measured from the displacements obtained by digital image correlation of subimages at the ends of the gage section. The applied strain rate was approximately 3.2×10^{-5} per second. Indicators in the form of short, extra-wide regions at each end of the gage section were included in the photolithographic design to assist in image correlation. Background correction and image smoothing of the digital images were used to minimize errors in the measured displacements.

From the slope of the measured displacement versus applied force, a value for Young's modulus E was calculated. Note that microtensile tests determine E for the in-plane direction of the film. Experiments were performed on four separate specimens and the results combined to obtain an average value for E. A measurement uncertainty of ±5% for this technique was obtained by analysis of the uncertainty budget and scatter in the individual measurements. The loading rates in the microtensile experiments were such that each load or unload cycle lasted approximately two minutes. Thus, these measurements were performed under quasistatic conditions.

C. Nanoindentation

Another section of the thin-film sample was evaluated by depth-sensing indentation, also known as nanoindentation. Nanoindentation timescales are similar to those for microtensile testing (i.e., quasistatic). Our indentation experiments were designed, performed, and analyzed using previously described methods.[5,10,11] A Berkovich geometry diamond indenter was used. The tip area function and frame compliance were determined using a two-reference-material method similar to that already published.[11] All displacements were corrected for the determined instrument frame compliance of 0.189 nm/mN. A simplified area function of the form $\sqrt{A_p} = 5.115\ h_c + 277$ was used, where A_p is the projected area of the indenter and h_c is the contact depth. It was found that this function was still valid at the indentation contact depths chosen ($h_c = 28$, 64, and 122 nm, corresponding to test forces of 0.3, 1, and 3 mN). The simplified area function deviated from the measured shape at the lowest indentation depth by less than 3%. Therefore, any resulting systematic underestimation of indentation modulus was less than 3%.

Ten indentations were performed at each test force and the values averaged. The indents were placed at 50 μm intervals to ensure that previous indentations did not affect subsequent results. In each indentation cycle, the maximum applied force was held for 60 s to allow time for the creep rate to reduce to sufficiently low levels. Thermal drift corrections were obtained for each experiment from a hold period of 60 s at the beginning of each indent experiment. The gradient of a linear fit to the last 40 s of the displacement-versus-time data measured during the hold period was used, in conjunction with the time recorded for each data point, to correct for the effect of thermal drift on the displacement values measured. Thermal drift rates were less than 0.03 nm/s. An additional hold period at 90% removal of applied force was used to check for residual uncorrected drift affecting the unloading curve.

Nanoindentation experiments determine values of the reduced modulus E_r of the system. The indentation modulus M of the sample was determined from the measured E_r through the relation

$$1/E_r = 1/M_{tip} + 1/M \quad , \tag{1}$$

where M_{tip} is the indentation modulus of the diamond tip. For an isotropic material $M = E/(1 - \nu^2)$, where E is Young's modulus and ν is Poisson's ratio. It is important to remember that nanoindentation (and atomic force acoustic microscopy) measurements are made in a direction perpendicular to the film plane, that is, in an out-of-plane direction. The values obtained by nanoindentation for a film/substrate system are a composite of the responses of both the film and substrate and therefore depend on depth. To determine the indentation modulus of the film independent of the substrate properties, a linear fit was applied to the plot of M versus a/t, where a is the radius of contact. The y intercept of this line, namely M for $a/t \to 0$, effectively gives M of the film alone.

D. Atomic force acoustic microscopy

Atomic force acoustic microscopy (AFAM) utilizes atomic force microscope (AFM) methods to determine nanoscale elastic properties.[12] Like nanoindentation, AFAM experiments determine values for the indentation modulus M; however, the lateral spatial resolution is higher. The AFAM technique consists of dynamically exciting the resonant modes of an AFM cantilever while it is in contact with a sample. The excitation amplitude is sufficiently small that the tip stays in contact with the sample throughout the measurements. The resonant frequencies of the cantilever are used to calculate the tip-sample contact stiffness and consequently the indentation modulus M from appropriate contact-mechanics models. The spatial resolution of AFAM is determined by the contact radius a between the sample and the AFM tip (typically, $a \sim 5$ to 20 nm.)

Our quantitative AFAM methods have been described in detail elsewhere.[13] The methods use a calibration sample whose indentation modulus M_{cal} has been determined independently. By comparing the contact-stiffness measurements for the unknown sample to those for the calibration sample, a value for M in the unknown material can be determined. This process avoids difficult tip characterization measurements and minimizes the effects

of tip wear.[12] For these experiments, we used a 1.5 mm thick piece of ⟨100⟩ single-crystal nickel as the calibration sample. A value $M_{cal} = M_{\langle 100 \rangle} = 219 \pm 2$ GPa was used for the calibration sample, based on pulse-echo ultrasonic measurements of the sample. The value of $M_{\langle 100 \rangle}$ is in excellent agreement with those predicted from literature values of the elastic moduli of single-crystal nickel.[14]

In this work, AFAM experiments were performed on the calibration sample and the Ni film sample in alternation. A total of six measurements on the calibration sample and five on the film sample were made at different positions. At each position, the frequencies of the cantilever's first two flexural modes were measured for three different static applied loads from approximately 0.9–2.6 μN. The contact-stiffness measurements for the Ni film sample were compared to those made on the calibration sample both immediately beforehand and afterwards. The resulting values of the indentation modulus obtained through this comparison were averaged to obtain a single value of M for the Ni film.

E. Surface acoustic wave spectroscopy

The thin-film sample was also investigated with surface acoustic wave (SAW) spectroscopy methods. In these experiments, high-frequency (~20–300 MHz) SAWs were generated by a pulsed laser and propagated across the sample surface. The detected SAW displacements as a function of propagation distance were used to calculate the phase velocity versus frequency, that is, the dispersion relation. Experiments were performed on both a commercial system with a piezoelectric detector[15] and a laboratory apparatus with a Michelson interferometer as detector.[16] It should be noted that the SAW spectroscopy method interrogates a sample area of a few square centimeters. Therefore, the results obtained represent the average properties of a macroscopic region of the sample.

Eleven dispersion relations were acquired corresponding to SAW propagation in one ⟨100⟩ and two ⟨110⟩ directions in the Si substrate. To analyze the data, the measured dispersion relations were compared to those predicted for SAW propagation in a film on a single-crystal Si substrate. For data analysis, we used a Green's-function approach to solve the inverse problem.[16,17] With this approach, the film and substrate can be modeled as either elastically isotropic or anisotropic, and the corresponding properties determined. The quoted SAW results represent the average and standard deviation calculated by analyzing each dispersion relation separately.

It is important to realize that several film properties can be determined from SAW spectroscopy data: elastic moduli, thickness, and density. This is because SAW propagation in a layered system, and consequently the SAW dispersion relation, is affected by all of these parameters to some extent. The number of parameters that can be determined from a given SAW dispersion relation depends on its specific frequency dependence.[15,17] Typically, values for only one or two parameters can be obtained. Input values for the remaining parameters must be provided, using either literature values or values obtained from independent measurements. To analyze the SAW spectroscopy data for the Ni film sample, we first assumed an isotropic model for the film properties and inverted the dispersion relations to determine the best-fit value for Young's modulus E. In this analysis, the following values were assumed: thickness $t = 772$ nm, density $\rho = 8.9$ g/cm^3, and Poisson's ratio $\nu = 0.3$. The values for ρ and ν were based on literature values for bulk nickel. As discussed below, we also analyzed the SAW dispersion relations to determine values for the density of the film. In this case, we used as input for the SAW analysis the elastic properties determined by AFAM, nanoindentation, and microtensile testing.

III. RESULTS AND DISCUSSION

A. Comparison of results

Table I contains the results obtained by all four techniques for the properties of the Ni film. An immediate conclusion that can be drawn from Table I is that the two direct measurements of M by different techniques, nanoindentation and AFAM, are in excellent agreement (difference approximately 1%). This demonstrates the validity of AFAM as a quantitative method in spite of its relative newness. The uncertainty in the AFAM result is larger than desired (~10–15 %), but is typical of AFAM measurements.[12,13] From previous experience with a variety of materials, we believe that the uncertainty is primarily caused by instrumentation and measurement issues such as tip wear and small variations in the tip-sample contact. We are working to improve our experimental techniques to reduce such contributions to the uncertainty.

Because AFAM and nanoindentation methods probe different material length scales, such agreement might be surprising. Nanoindentation yields an effective value representative of many grains, while AFAM senses the properties of only a few grains. However, the microstructure of our Ni film was uniform and strongly textured. In a highly textured film, all of the grains yield roughly similar values for M. Therefore the average AFAM value is close to the average nanoindentation results extrapolated to $a/t = 0$.

In contrast to the AFAM and nanoindentation results for the indentation modulus, the results for Young's modulus obtained by microtensile testing and SAW spectroscopy differ significantly (~15%). Both methods yield macroscopic material properties, so it is unlikely that the discrepancy is due to length-scale effects. The reduced

TABLE I. Experimental and theoretical results for the Young's modulus *E,* indentation modulus *M,* and density ρ of a Ni film 772 nm thick. Analysis of the SAW spectroscopy data to obtain *E* assumed that the film density ρ = 8.9 g/cm^3 and Poisson's ratio n = 0.3. Values in the "calculated" column were obtained by assuming reduced values for the cubic elastic moduli of single-crystal Ni as described in the text, in order to include nanocrystalline effects. Two different sets of values for *M* and *E* were calculated by assuming that the film was either elastically isotropic or anisotropic (transversely isotropic). Different values for ρ were obtained from the SAW spectroscopy data, depending on the elastic model used.

		Value		
			Calculated	
Property	Method	Measured	Isotropic	Anisotropic
E (GPa)	Microtensile	177 ± 10	187.9	178.4
	SAW spectroscopy	204 ± 8		
M (GPa)	Nanoindentation	220 ± 10	207.2	221.4
	AFAM	223 ± 28		
ρ (g/cm^3)	SAW spectroscopy	8.79 ± 0.10 (isotropic) 8.74 ± 0.10 (anisotropic)	8.90 (bulk, literature)	

value of *E* obtained by microtensile testing is consistent with previous results on Ni and other films.[18,19] Nanoindentation and microtensile results were previously compared for Ni films made by the LIGA electrodeposition process.[19] Films were about 500 times thicker (~400 μm) but yielded results virtually identical to ours. In that work, values of $M = 219 \pm 15$ GPa by use of nanoindentation and $E = 178 \pm 14$ GPa by use of microtensile testing were obtained for one sample.

Possible reasons given in Ref. 19 for this discrepancy included indenter pileup effects that could increase nanoindentation values and film porosity that could lower microtensile values. Cross-sectional SEM images like that in Fig. 2(a) did not reveal the presence of closed pores in this film. AFAM does not plastically deform the sample, and its value for *M* is in excellent agreement with our nanoindentation value. Therefore we believe that our measured nanoindentation value is not significantly affected by pileup. Furthermore, previous nanoindentation studies[20] suggest that the method used here to obtain *M* is relatively immune to the effects of pileup. It was found that by extrapolating to $a/t = 0$, a value for *M* in the film material could be obtained. Other work on the same films[21] showed that pileup is not visible for shallow indents but is progressive with indentation depth. This would also imply that the extrapolation method would act to minimize the effect of pileup on the intercept value.

On the other hand, the value of *E* determined from SAW spectroscopy is highly dependent on the values of other film parameters used in the data analysis. We assumed bulk literature values for ρ and ν, but the film's actual values could differ. To examine how the SAW results depend on different film parameters, we modeled an isotropic film with $d = 772$ nm, $E = 204$ GPa, $\nu = 0.3$, and ρ = 8.9 g/cm^3 on (001) Si. If ρ was reduced by 1% in this system, it was necessary to decrease *E* by 3.1% to obtain the same SAW dispersion relation. Thus, if the actual film density was lower than the assumed (bulk) value by only a few percent, the SAW result for *E* would be lower by several percent and therefore more consistent with the microtensile results. Furthermore, the SAW analysis model assumed an elastically isotropic film, contrary to the evidence obtained by x-ray diffraction. The disagreement between SAW and microtensile results may therefore be misleading. We will show in the next section that by using an elastically anisotropic model for the film's properties, all of the results can be interpreted in a self-consistent way.

Further examination of Table I also reveals that all of the experimental values are noticeably lower than those predicted from the literature. The values $C_{11} = 249.0$ GPa, $C_{12} = 152.7$ GPa, and $C_{44} = 118.9$ GPa represent average literature values for the single-crystal cubic elastic moduli C_{ij} of nickel.[14] With Voigt–Reuss–Hill methods, the elastic properties of randomly-oriented, polycrystalline nickel can be calculated from these values.[22] Using the above values for C_{ij}, we predict $E = 216.0$ GPa and $\nu = 0.305$. From the relationship $M = E/(1 - \nu^2)$ for an isotropic material, these values of *E* and ν yield $M = 238.2$ GPa. Thus, the measured values in Table I are 6–18% lower than expected for isotropic, polycrystalline nickel.

Using reduced values of C_{ij}, we repeated our calculations of *E* and *M*. Without a compelling reason to adjust the different moduli independently, we chose to reduce the values of all the C_{ij} by the same relative fraction. Reducing the C_{ij} to 87% of the bulk single-crystal values given above yielded the best agreement with all of the measured values at the same time. The values calculated for *E* and *M* with the reduced moduli are shown in the "isotropic" column in Table I. They are approximately 6% higher and lower, respectively, than the measured values of *E* (microtensile) and *M* (nanoindentation and AFAM). Out of curiosity, we also adjusted the values of each C_{ij} separately in an effort to achieve better

agreement between the measured and calculated values. We could not find a combination that simultaneously matched both E and M, assuming elastic isotropy.

Reduced values of thin-film elastic moduli, particularly in nanocrystalline materials, have been observed and discussed by several authors.[18,23,24] The discrepancy between the measured values and those predicted from bulk values is usually attributed to film porosity[23] or some type of grain-boundary effect. Possible intercrystalline effects include incomplete cohesion or "microcracking" at the grain boundaries[18] and an increased volume fraction of triple junctions.[24] Such effects lead to reduced stiffness in the intercrystalline material. Using the model described in Ref. 24 and assuming an average grain diameter $d = 27$ nm, we calculated that the volume fraction of intercrystalline (grain-boundary and triple-junction) material in this film was approximately 11%. Therefore, the volume fraction of intercrystalline material is substantial and intercrystalline effects might explain the observed reduction in elastic properties.

The reduced-modulus values obtained in the data analysis can be justified by considering models for nanocrystalline materials.[24,25] We calculated effective values of the cubic elastic moduli C_{ij}^{eff} for a composite system containing nanoscale Ni grains and intercrystalline material. We assumed that the volume fraction of intercrystalline material was 11% and that the elastic moduli of the intercrystalline material were 0.33 times that of the single-crystal values C_{ij}.[25] By a simple rule-of-mixtures weighting, we calculated $C_{ij}^{eff} = 0.92C_{ij}$. This agrees quite well with the value obtained in our data analysis (0.87), given the relatively simple nature of our calculations.

B. Transversely isotropic model for elastic properties of the film

The "isotropic" entries in Table I obtained with reduced-modulus values agree more closely with our measurements than those predicted from single-crystal values. However, they still differ from the measurements by more than the measurement uncertainty in some cases. Therefore, we now present a second way to interpret our measurements, which takes into account the anisotropy of the film's elastic properties. Since the anisotropy factor $\eta = 2\,C_{44}/(C_{11} - C_{12})$ is relatively large for nickel ($\eta \approx 2.5$), it is possible that small deviations from uniform texture might affect the elastic properties of the film. X-ray analysis indicated a preferred $\langle 111 \rangle$ orientation, as is the case for many films. The simplest anisotropic model for the elastic properties of such a film is transverse isotropy, in which the properties are isotropic or rotationally invariant in the plane of the film but differ from the out-of-plane properties.

Transverse elastic isotropy is equivalent to hexagonal symmetry, which has five independent elastic stiffness moduli: c_{11}, c_{12}, c_{13}, c_{33}, and c_{44}. To describe a $\langle 111 \rangle$-oriented polycrystalline Ni film with hexagonal elastic symmetry, the cubic single-crystal moduli C_{ij} were first rotated so that the $\langle 111 \rangle$ direction was perpendicular to the plane of the film. This process resulted in a set of elastic stiffness moduli c_{ij} with hexagonal symmetry. The rotated c_{ij} were then averaged over all directions in the plane of the film, that is, the (111) plane, to obtain the final averaged hexagonal moduli $\langle c_{ij} \rangle$. The mathematical steps to perform the above process are widely available in the literature (see, for instance, Ref. 26). The $\langle c_{ij} \rangle$ used in our calculations were the Voigt–Reuss–Hill average values. Voigt values were obtained by rotating and averaging the cubic stiffness tensor C_{ij} as described above. The Reuss values were obtained by performing the same process to the corresponding elastic compliance tensor S_{ij}.

With transversely isotropic elastic symmetry, the in-plane Young's modulus is given by $E = 1/\langle s_{11} \rangle$, where $\langle s_{11} \rangle$ belongs to the hexagonal elastic compliance tensor $\langle s_{ij} \rangle$. In terms of the hexagonal elastic stiffness moduli $\langle c_{ij} \rangle$

$$E = 1/\langle s_{11} \rangle = \frac{\langle c_{33} \rangle (\langle c_{11} \rangle^2 - \langle c_{12} \rangle^2) - 2\langle c_{13} \rangle^2 (\langle c_{11} \rangle - \langle c_{12} \rangle)}{\langle c_{33} \rangle (\langle c_{11} \rangle^2 - \langle c_{13} \rangle^2)} . \quad (2)$$

The calculation and interpretation of indentation modulus values for anisotropic materials is more complicated than the corresponding isotropic case.[27] However, analytical expressions have been derived to calculate the out-of-plane indentation modulus M for transversely isotropic materials.[27,28] These expressions are not repeated here for the sake of brevity.

Using this transversely isotropic model for the elastic properties of the Ni film, we calculated values for E and M. As before, the predicted values were significantly greater than the measured ones if bulk values for C_{ij} were used ($M = 249.3$ GPa and $E = 240.6$ GPa). Reducing all of the values of C_{ij} by the same fraction provided better agreement with the measured values of M and E simultaneously. The best agreement with the AFAM and nanoindentation measurements were achieved by reducing all of the C_{ij} to 89% of their bulk literature values to obtain $M = 221.9$ GPa for the out-of-plane indentation modulus. The agreement between the calculated and measured values, especially for the microtensile result, was improved further by adjusting the values of $\langle c_{ij} \rangle$ individually. Changes in $\langle c_{11} \rangle$ had the most effect on the relative values of E, but virtually no effect on M. The values in the "anisotropic" column of Table I were calculated by first reducing all the C_{ij} to 90% of their bulk literature values and then performing the rotation and averaging processes described above to obtain a set of

$\langle c_{ij} \rangle$. Finally, we fixed $\langle c_{11} \rangle = 248$ GPa and the values of E and M were calculated. Agreement with all of the measured values is excellent (less than 1% and within experimental uncertainty). Analogous to the discussion above for the isotropic case, the reduced values for the elastic properties needed to match the data can be interpreted as effective values for a composite system of nanocrystallites and one or more reduced-modulus intercrystalline phases. The additional reduction of the in-plane modulus $\langle c_{11} \rangle$ might indicate differences between the anisotropy of a bulk material and of a film created under these growing conditions.

SAW dispersion relations are typically used to determine a film's elastic properties, but in this case the elastic properties had already been evaluated in several ways. We therefore analyzed the SAW data to obtain the film density ρ. This approach also illustrates how results from a suite of complementary methods can be combined to obtain more complete information about the entire set of film properties. For both the isotropic and anisotropic models described above, a best-fit value for ρ was determined assuming the reduced C_{ij} given above and the SEM value for t. We discussed above how reducing the assumed (input) value for ρ lead to reduced values for C_{ij} in the SAW analysis. In a similar way, reduced values for C_{ij} are expected to yield lower predicted values for ρ. This behavior is due to the relationship between C_{ij} and ρ in expressions for the SAW velocity.

The values of ρ determined from analysis of the SAW spectroscopy data are shown in Table I. For both the isotropic and anisotropic models, the values of ρ were only 1–2% less than $\rho_{bulk} = 8.90$ g/cm^3 for bulk Ni.[14] These results are consistent with predictions of nanocrystalline models. We assumed that the volume fraction of the intercrystalline material was 11% and that the density of this material was 0.82 times that of the crystalline material.[25] With these values, a rule-of-mixtures calculation yields $\rho_{eff} = 0.98\ \rho_{bulk}$ for the nanocrystalline film, in good agreement with our results.

C. Additional nanocrystalline Ni thin-film specimens

Two additional Ni film/Si substrate samples prepared in the same manner were also evaluated. Values for the film thickness t and average grain diameter d are shown in Table II. Nanoindentation and microtensile experiments were not performed on these samples because they were so thin. However, AFAM and SAW spectroscopy methods were readily applied. The experimental results for all three samples are given in Table II. It can be seen that the AFAM values for M were identical within measurement uncertainty to those obtained on the 772-nm film. Thus, even for a film only several tens of nanometers thick, the influence of substrate properties on AFAM measurements of M was negligible (for this particular film/substrate combination).

TABLE II. Experimental results for three nanocrystalline Ni thin films. Shown are values for the film thickness t and average grain diameter d determined by SEM, the indentation modulus M_{AFAM} determined by AFAM, and the film density ρ determined by SAW spectroscopy.

t (nm)	d (nm)	M_{AFAM} (GPa)	ρ_{SAW} (g/cm^3)
772 ± 5	27 ± 10	223 ± 28	8.79 ± 0.10
204 ± 4	22 ± 5	220 ± 19	8.72 ± 0.04
53 ± 2	16 ± 6	210 ± 26	8.59 ± 0.10

SAW dispersion relations were obtained for these samples (eight for the 204 nm film sample and six for the 53 nm film sample). For each film, reduced values of the cubic moduli C_{ij} for single-crystal Ni were first determined from the AFAM measurement of M by use of an isotropic model for the film's elastic properties. Values for C_{ij} that were 88–93% of the literature bulk values provided the closest agreement with M. These values of C_{ij} and the SEM values for t were used as input in the SAW data analysis to obtain the best-fit value of ρ for each film from the dispersion relations. Like the first (thickest) film, the values of ρ obtained for the two thinner films were only slightly lower (2–4%) than the literature value for bulk Ni. From the measured values of d for each film, we estimated the volume fraction of intercrystalline material in each film and the corresponding reduction in density predicted by the nanocrystalline models mentioned above. The predicted reductions in density were approximately 2–3%, consistent with those obtained in the SAW analysis.

The analysis approach described above forms the basis for a model that combines elastic anisotropy and nanocrystalline effects in thin films. Development of this model requires further calculations, for instance of anisotropic relations in nanocrystalline materials and their effect on parameters such as the modulus reduction factor for the intercrystalline phases. In addition, the validity of the models could be experimentally tested more effectively using films with smaller grain diameter than studied here ($d \sim 15$ nm or less). In such films, the volume fraction of intercrystalline material expected to be more significant.

IV. SUMMARY AND CONCLUSIONS

The properties of nanocrystalline nickel thin films were evaluated using several measurement methods. The sample area interrogated by each method ranged from macroscale (SAW spectroscopy) through intermediate regimes (microtensile testing and nanoindentation) to the nanoscale (AFAM). Measurements of the same elastic property (M) obtained by two very different methods, AFAM and nanoindentation, were in excellent agreement.

In contrast, results for different elastic properties (E and M) obtained by different methods initially did not seem self-consistent. The disparate results were better reconciled with a transversely isotropic model for the film's elastic properties.

However, all of the results were lower than expected for bulk, polycrystalline nickel. To match the experimental results with either an isotropic or anisotropic model for the film's elastic properties, it was necessary to reduce the modulus values used by approximately 10% from the single-crystal values. This reduction in modulus was shown to be consistent with a nanocrystalline film structure containing a significant volume fraction of grain-boundary or other intercrystalline material. SAW spectroscopy results indicated that the film density was only a few percent less than the bulk value, also consistent with simple nanocrystalline models. Additional test on films approximately 200 and 50 nm thick yielded similar results. These results illustrate a relatively straightforward way to interpret mechanical-property measurements of thin films that is based on a more physically realistic model than the simple assumption of elastic isotropy. Such an approach should prove valuable as the importance of accurately understanding and predicting thin-film behavior continues to increase.

ACKNOWLEDGMENTS

We thank W.H. Rippard and S.E. Russek, National Institute of Standards and Technology (NIST), for fabricating the Ni thin-film samples, and S. Hirsekorn (Fraunhafer Institute for Nondestructive Testing) for calculating the indentation moduli of single-crystal Ni. We are grateful to J. Vlassak (Harvard University) for valuable discussions.

REFERENCES

1. F.R. Brotzen: Mechanical testing of thin films. *Int. Mater. Rev.* **39,** 24 (1994).
2. O. Kraft and C.A. Volkert: Mechanical testing of thin films and small structures. *Adv. Eng. Mater.* **3,** 99 (2001).
3. A.G. Every: Measurement of the near-surface elastic properties of solids and thin supported films. *Meas. Sci. Technol.* **13,** R21 (2002).
4. K.F. Badawi, P. Villain, Ph. Goudeau, and P-O. Renault: Measuring thin film and multilayer elastic constants by coupling in situ tensile testing with x-ray diffraction. *Appl. Phys. Lett.* **80,** 4705 (2002).
5. N.M. Jennett, G. Aldrich-Smith, and A.S. Maxwell: Validated measurement of Young's modulus, Poisson ratio and thickness for thin coatings by combining instrumented nanoindentation and acoustical measurements. *J. Mater. Res.* **19,** 143 (2004).
6. T.E. Buchheit, D.A. LaVan, J.R. Michael, T.R. Christenson, and S.D. Leith: Microstructural and mechanical properties investigation of electrodeposited and annealed LIGA nickel structures. *Metall. Mater. Trans. A* **33A,** 539 (2002).
7. A. Robertson, U. Erb, and G. Palumbo: Practical applications for electrodeposited nanocrystalline materials. *Nanostruct. Mater.* **12,** 1035 (1999).
8. Y. Choi and S. Suresh: Size effects on the mechanical properties of thin polycrystalline metal films on substrates. *Acta Mater.* **50,** 1881 (2002).
9. D.T. Read, Y-W. Cheng, R.R. Keller, and J.D. McColskey: Tensile properties of free-standing aluminum thin films. *Scripta Mater.* **45,** 583 (2001).
10. BS EN ISO 14577:2002 parts 1–3, Metallic Materials—Instrumented Indentation Test for Hardness and Materials Parameters (International Organization for Standardization, Geneva, Switzerland).
11. K. Herrmann, N.M. Jennett, W. Wegener, J. Meneve, K. Hasche, and R. Seemann: Progress in determination of the area function of indenters used for nanoindentation. *Thin Solid Films* **377–378,** 394 (2000).
12. U. Rabe, S. Amelio, M. Kopycinska, S. Hirsekorn, M. Kempf, M. Göcken, and W. Arnold: Imaging and measurement of local mechanical material properties by atomic force acoustic microscopy. *Surf. Interface Anal.* **33,** 65 (2002).
13. D.C. Hurley, K. Shen, N.M. Jennett, and J. Turner: Atomic force acoustic microscopy methods to determine thin-film elastic properties. *J. Appl. Phys.* **94,** 2347 (2003).
14. G. Simmons and H. Wang: *Single Crystal Elastic Constants and Calculated Aggregate Properties: A Handbook,* 2nd ed. (MIT Press, Cambridge, MA, 1971), pp. 56–58.
15. D. Schneider, T. Schwarz, and B. Schultrich: Determination of elastic modulus and thickness of surface layers by ultrasonic surface waves. *Thin Solid Films* **219,** 92 (1992).
16. D.C. Hurley, V.K. Tewary, and A.J. Richards: Surface acoustic wave methods to determine the anisotropic elastic properties of thin films. *Meas. Sci. Technol.* **12,** 1486 (2001).
17. V.K. Tewary: Theory of elastic wave propagation in anisotropic film on anisotropic substrate: TiN film on single-crystal Si. *J. Acoust. Soc. Am.* **112,** 925 (2002).
18. H. Huang and F. Spaepen: Tensile testing of free-standing Cu, Ag, and Al thin films and Ag/Cu multilayers. *Acta Mater.* **48,** 3261 (2000).
19. S. Stauss, P. Schwaller, J-L. Bucaille, R. Rabe, L. Rohr, J. Michler, and E. Blank: Determining the stress-strain behaviour of small devices by nanoindentation in combination with inverse methods. *Microelectron. Eng.* **67–8,** 818 (2003).
20. European report: INDICOAT SMT-CT98-2249, NPL Report MATC (A) 24 (National Physical Laboratory, Middlesex, U.K., 2001).
21. I. Spary, N.M. Jennett, and A.J. Bushby: Indentation and finite element modeling investigations of the indentation size effect in aluminum coatings on borosilicate glass substrates, in *Thin Films—Stresses and Mechanical Properties X*, edited by S.G. Corcoran, Y-C. Joo, N.R. Moody, and Z. Suo (Mater. Res. Soc. Symp. Proc. **795,** Warrendale, PA, 2004), p. 455.
22. G. Grimvall: *Thermophysical Properties of Materials* (Elsevier, New York, 1999).
23. P. Sanders, C.P. Youngdahl, and J.R. Weertman: The strength of nanocrystalline metals with and without flaws. *Mater. Sci. Eng. A* **234–236,** 77 (1997).
24. G. Palumbo, S.J. Thorpe, and K.T. Aust: On the contribution of triple junctions to the structure and properties of nanocrystalline materials. *Scripta Metall. Mater.* **24,** 1347 (1990).
25. G-F. Wang, X-Q. Feng, S-W. Yu, and C-W. Nan: Interface effects on effective elastic moduli of nanocrystalline materials. *Mater. Sci. Eng. A* **363,** 1 (2003).
26. E. Anastassakis and M. Siakavellas: Elastic properties of textured diamond and silicon. *J. Appl. Phys.* **90,** 144 (2001).
27. J.J. Vlassak and W.D. Nix: Indentation modulus of elastically anisotropic half spaces. *Philos. Mag. A* **67,** 1045 (1993).
28. G.M.L. Gladwell: *Contact Problems in the Classical Theory of Elasticity* (Sijthoff and Noordhoff, Germantown, MD, 1980), p. 581.